Title
Inhomogeneous Surface Diffusion for Image £ltering

Journal
Pattern Recognition Letters, 8

Authors
Ford, Gary
El-Fallah, Adel

Publication Date
1997

Peer reviewed

Inhomogeneous Surface Diffusion for Image Filtering

Gary E. Ford and Adel I. El-Fallah
CIPIC, Center for Image Processing and Integrated Computing
University of California, Davis
Davis, CA 95616

Abstract

Most of the recent work on inhomogeneous diffusion in image filtering focuses on diffusing the isotope curve. We present a less familiar approach to the development of inhomogeneous diffusion algorithms in which the image is regarded as a surface in three-space. The magnitude of the surface normal controls a diffusion that evolves the image surface at a speed proportional to its mean curvature. A discrete algorithm to implement this proposed diffusion is introduced and we show experimentally that the algorithm develops singularities that reveal, preserve, and enhance the underlying signal. If the input signal is an isolated noisy edge, this leads to complete noise removal and enhancement without affecting the edge locality.

1 Introduction

Methods of geometry-driven diffusion for image filtering are often based on analogy to the diffusion of heat. Perona and Malik [1] argued that the conduction coefficient in the heat equation, which is space invariant in the classic theory, should be allowed to vary spatially. They provided a mathematical foundation for the concept of selective smoothing. More recent work on inhomogeneous diffusion in image filtering has focused on diffusing the isotope curve, and is based on a level function or curve diffusion setting [2–6].

We present a less familiar approach to the development of inhomogeneous diffusion (ID) algorithms in which the image is regarded as a surface in three-space. The approach we describe is also related to the Perona and Malik anisotropic diffusion model [1], but rather than viewing the model

as a differential equation in terms of the image intensity, we propose a *surface diffusion* model in which the surface itself is diffused. We show in Section 2 that this is accomplished by introducing a function that *implicitly* represents the surface. We then introduce a diffusion that relates the magnitude of the surface normal to surfaces evolving at a speed proportional to the mean curvature of the image surface. We also compare this diffusion to homogeneous diffusion. There has been a surge of interest in anisotropic diffusion (see e.g., [7]), and in Section 3 we review some of the related diffusions and compare them to our proposed framework. The properties of the proposed diffusion interpreted geometrically are further discussed in Section 4. The details of the discrete implementation of a two-dimensional algorithm are described in Section 5. The evolution of the noise free and noisy edge are presented experimentally in Section 6. Examples of applications to image noise removal and transparent coding are given in Section 7.

2 Theory of Image Surface Mean Curvature Diffusion

2.1 The Surface Representation

By introducing the third coordinate of space z and assigning the image intensity to this coordinate, the image can be characterized by

$$g\left(x, y, z\right) = z - I\left(x, y\right) , \tag{1}$$

and the surface $\mathcal{S}$ is said to be defined by

$$\mathcal{S} \; : \; g\left(x, y, z\right) = 0. \tag{2}$$

The differential of g never vanishes, so the surface represented by g always exists [8]. The surface gradient ∇g has magnitude

$$|\nabla g| = \sqrt{1 + I_x^2 + I_y^2} , \tag{3}$$

and the *unit* normal vector field of the surface is

$$\mathcal{N} = \frac{\nabla g}{|\nabla g|} = \left(\frac{-I_x}{\sqrt{I_x^2 + I_y^2 + 1}}, \frac{-I_y}{\sqrt{I_x^2 + I_y^2 + 1}}, \frac{1}{\sqrt{I_x^2 + I_y^2 + 1}} \right) , \tag{4}$$

2.2 Mean Curvature Diffusion

The diffusion of g is modeled by

$$\frac{\partial g}{\partial t} = \nabla \bullet (\mathrm{C}\, \nabla g) \tag{5}$$

and we are interested in an inhomogeneous diffusion in which the diffusion coefficient is the inverse of the surface gradient magnitude

$$\mathrm{C} = \frac{1}{|\nabla g|} \tag{6}$$

This leads to the diffusion rate

$$\frac{\partial g}{\partial t} = \nabla \bullet \mathcal{N} = -\frac{\partial}{\partial x}\left(\frac{I_x}{\sqrt{I_x^2 + I_y^2 + 1}}\right) - \frac{\partial}{\partial y}\left(\frac{I_y}{\sqrt{I_x^2 + I_y^2 + 1}}\right). \tag{7}$$

The first term on the right is the normal curvature in the x direction and the second term is the normal curvature in the y direction. The *mean curvature* H is the average value of the normal curvature in *any* two orthogonal directions and thus

$$\frac{\partial g}{\partial t} = 2\mathrm{H} = \frac{I_{xx}\left(1 + I_y^2\right) - 2 I_{xy} I_x I_y + I_{yy}\left(1 + I_x^2\right)}{|\nabla g|^3} \tag{8}$$

Thus, the image surface diffuses at a rate equal to twice the mean curvature and thus, this process is known as *mean curvature diffusion* (MCD).

2.3 Relationship to Homogeneous Diffusion

In homogeneous diffusion, the diffusion coefficient C in (5) is constant and the diffusion equation becomes

$$\frac{\partial g}{\partial t} = \nabla^2 g \tag{9}$$

where the Laplacian $\nabla^2 g$ is the divergence of the gradient of g. From the analysis given in [9], the diffusion rate is

$$\frac{\partial g}{\partial t} = \frac{\partial^2 g}{\partial n^2} + |\nabla g|\,(2\mathrm{H}), \tag{10}$$

where n is a coordinate in the direction of the surface normal. Thus, homogeneous diffusion is seen to depend on the divergence in surface magnitudes represented by $\frac{\partial^2 g}{\partial n^2}$ and $|\nabla g|$, as well as

the mean surface curvature, H. This is in contrast to the inhomogeneous diffusion of (8), which by averaging only H, a divergence in direction that is void of magnitudes, preserves the underlying signal that is characterized by divergences in magnitude.

3 Related Diffusions

3.1 Curve Diffusions

Recent work on geometric diffusions in image filtering has focused on diffusing the isotope curve, $I(x, y) =$ constant. The motivation has been to smooth the tangent to the isotope, thereby preserving it. One diffusion model that has been suggested [2] reduces in the limit (of scale space) to a diffusion rate

$$\frac{\partial I}{\partial t} = \hat{\kappa} = \frac{I_{xx} I_y^2 - 2 I_{xy} I_x I_y + I_{yy} I_x^2}{|\nabla I|^3} \tag{11}$$

where $\hat{\kappa}$ is the curvature of the isotope and $|\nabla I|^2 = I_x^2 + I_y^2$. Complete analysis was provided which shows the existence and uniqueness of the solution of the associated differential equation. This analysis and the obtained results assume that the gradients are obtained after Gaussian smoothing. In another approach [4], minimizing the functional $\int\int \sqrt{I_x^2 + I_y^2}\, \mathrm{d}x\, \mathrm{d}y$, led to the diffusion in (11). Note that if the surface area functional $\int\int \sqrt{1 + I_x^2 + I_y^2}\, \mathrm{d}x\, \mathrm{d}y$ is minimized, then it is simple to show that the proposed diffusion in (8) arises. Other work based on the level function or curve diffusion setting include [5, 6].

3.2 Eulerian Viewpoint, Viscosity Solutions

The isotope curve diffusions were motivated by recent work [10] which introduces a weak solution for a diffusion related to (11) in arbitrary dimensions. This work was inspired by the earlier works on viscosity solutions of nonlinear partial differential equations [11–13]. The main difficulty of this approach occurs when ∇I vanishes and (11) becomes undefined. This equation must then be interpreted in some weak sense as in [10].

3.3 Lagrangian Viewpoint, Differential Geometry

The Lagrangian approach is based on classical differential geometry mappings or parameterizations. In this approach the image is a classic Monge surface represented by the tip of the position vector

$\mathbf{r}(x, y) = (x, y, I(x, y))$. Mean curvature flows from this viewpoint have been studied [14, 15] and the short time existence of these mappings have been established [16]. The main problem with the mapping approach is the difficulty of handling topological changes, such as the development of singularities, which are bound to form as the surface evolves and which cannot be directly studied by the motion equation derived from the mapping [17]. Ecker and Huisken [14] characterized the longtime behavior of entire graphs of controlled growth of the motion

$$\frac{\partial \mathbf{r}}{\partial t} = (\mathrm{H})\ \mathbf{n}\,, \tag{12}$$

where $\mathbf{n}$ is the unit surface normal vector. In a study of the local properties of the flow in (12), they were able to obtain regularity estimates which are interior both in space and time [15]. As a consequence they were able to obtain a short time existence result assuming only a uniform local Lipschitz condition for the initial surface. They also proved a general maximum principle for the associated parabolic equations, and as an application of this maximum principle they showed that nonnegative mean curvature is preserved by (12) under reasonably weak conditions. They also deduced that if the initial surface is a locally Lipschitz continuous entire graph over R^n, then the mean curvature flow of (12) has a smooth solution with the initial data which exists for all time.

3.4 Proposed Approach: Surface Motion

Our proposed approach is a surface motion approach in contrast with the level function approach discussed in Sections 3.1 and 3.2. The proposed MCD can be related to the Lagrangian viewpoint of parametric mapping of Section 3.3. We can show this relationship by tracking the point $(\mathbf{r}, t)$ *on* the surface. Straightforward analysis shows that the motion for MCD, up to tangential diffeomorphism is equivalent to

$$\frac{\partial \mathbf{r}}{\partial t} = -\frac{2\mathrm{H}}{|\nabla g|}\mathbf{n} \tag{13}$$

Thus MCD is very close to the motion in (12).

4 Properties of Mean Curvature Diffusion

4.1 Edge Invariance

An important image structure, the edge, can be shown to be invariant to mean curvature diffusion. To demonstrate this invariance consider the Gaussian blurred step edge of intensity 75 and a blurring standard deviation of 1.0, shown in Fig. 1. From (8), the diffusion rate for MCD is twice the mean curvature, and the mean curvature of the Gaussian blurred edge, computed from (8) and plotted in Fig. 1, is virtually constant and equal to zero over an interval centered on the edge location. As a result, the image intensity at the edge remains unchanged under MCD, as desired. The width of the zero interval offers a desired numerical stability. In contrast, homogeneous diffusion (10) is driven by the Laplacian, which has only a zero crossing with steep slope at the edge location, and with a magnitude that is much larger than the mean curvature. This leads to strong changes in image intensity across the edge.

[Figure 1 about here.]

4.2 Basic Strategy–Iterative Averaging in the Small

The visual information in the intensity image $I(x, y)$ is characterized by the geometry of the surface: edges, lines, corners, etc. This geometry for most images is more complex than lines and/or corners. Algorithms which detect and separately process each structural type are often complex and inefficient. Our approach offers an alternative, by observing that even for complex geometry, any surface *locally* is a plane having zero mean curvature. This implies that if MCD is applied "in the small" or on a small kernel then the image structure will be preserved. Thus, MCD will be implemented iteratively with a kernel of small spatial size (3×3). The need for iterative processing requires a careful explanation.

Our basic strategy is to locally render the geometric features invariant and then patch the local features by iterative averaging in order to capture the global geometry. The iterative processing will follow the rotations and turns of the local planes. Similarly, curves, which *locally* are line segments, will remain intact under MCD. At larger spatial scales, the variation in line orientation will be captured by the iterative averaging that brings more spatial context to bear on the averaging process. Thus, the spatial extent of the filter is proportional to the number of iterations (time).

This iterative averaging with a small kernel leads to less interaction of nearby structures (edges) than does non-iterative averaging with a larger kernel.

4.3 MCD Stability

The diffusion coefficient of MCD is

$$C = \frac{1}{|\nabla g|} = \frac{1}{\sqrt{1 + |\nabla I|^2}} \,. \tag{14}$$

and the diffusion will be stable because this coefficient has a value in the interval [0,1]. This is in contrast to diffusions based on the coefficient $C = |\nabla I|^{-1}$, which is not defined where $|\nabla I|$ vanishes. A threshold must be set on this coefficient, introducing a discontinuity that results in a non-smooth filter.

In [18] it was shown that one-dimensional diffusion is well posed iff $\phi'(s) \geq 0$, where $\phi(s)$ is a flux function defined as $\phi(s) = s\,C(s)$. This condition was also used in [19]. Note that the proposed MCD coefficient in (14) satisfies this condition since $\phi'(s) = \left(1 + s^2\right)^{-\frac{3}{2}} > 0$.

5 Algorithm Simulation and Implementation

We are proposing the diffusion of (5) with the coefficient of (6) and by substituting for g using its definition in (1)

$$\frac{\partial z}{\partial t} - \frac{\partial I}{\partial t} = \nabla \bullet \left(\frac{\nabla z}{|\nabla g|}\right) - \nabla \bullet \left(\frac{\nabla I}{|\nabla g|}\right) \tag{15}$$

which shows that with the image regarded as a graph $z = I(x, y)$, it is sufficient to only implement

$$\frac{\partial I}{\partial t} = \nabla \bullet \left(\frac{\nabla I}{|\nabla g|}\right) \,, \tag{16}$$

in order to satisfy (15).

5.1 Discrete Realization

A one-dimensional ID is modeled by the equation

$$\frac{\partial I(x,t)}{\partial t} = \frac{\partial}{\partial x}\left[C(x,t)\frac{\partial I(x,t)}{\partial x}\right] \tag{17}$$

where $I(x,t)$ is the image being diffused, $I(x,0) = I_0(x)$ is the original image, and $C(x,t)$ is the conduction coefficient. By taking a Taylor series expansion of I, approximating by ignoring higher order terms, and approximating partial derivatives by first differences on three adjacent pixels x_{-1}, x_0, x_1, we obtain the iterative realization [8]

$$I(x_0,t) \approx \{.5C(x_{-1})I(x_{-1}) + [1 - .5C(x_{-1}) - .5C(x_1)]I(x_0) + .5C(x_1)I(x_1)\}_{t-1}. \quad (18)$$

5.2 Maximum (and Minimum) Principle, Causality, and Stability

The homogeneous diffusion equation satisfies the classical maximum (and minimum) principle, which states that the maximum (minimum) occurs either at time zero or at the boundary, as long as the evolution is forward in time [20]. This ensures stability, and is sometimes referred to as the *causality* criterion since no new maxima or minima occur in the interior as we evolve in time. We will now show that the realization derived in the previous subsection also satisfies the maximum (minimum) principle provided that the diffusion coefficient $C(x,t)$ satisfies the simple condition: $0 \leq C(x,t) \leq 1$.

From (18) we have

$$I(x_0,t) \leq \{I_{max}\}_{t-1} \{.5C(x_{-1}) + [1 - .5C(x_{-1}) - .5C(x_1)] + .5C(x_1)\}_{t-1} = \{I_{max}\}_{t-1}, \quad (19)$$

where $\{I_{max}\}_{t-1}$ is the maximum value of $I(x,t-1)$. Note that the inequality is true if $C(x_{-1}) \geq 0$, $C(x_1) \geq 0$, and $[1 - .5C(x_{-1}) - .5C(x_1)] \geq 0$. These inequalities are satisfied if $0 \leq C(x_i) \leq 1$ for all i. Similarly one can show that no new minima will be created if the same condition is satisfied, thus this is the *only* condition we have to impose to guarantee the stability of the realization.

5.3 Two Dimensional Inhomogeneous Diffusion Algorithm

A two dimensional diffusion algorithm results from a natural extension of the kernel given in (18). The Sobel operator [21] is chosen to estimate $|\nabla I|$ and to implicitly remove noise (point to point fluctuation). It was chosen because it is a difference of averages operator and because its response to a diagonal edge is better than that of other difference of averages operators. The algorithm follows.

1. Apply the Sobel operator to the current image to compute estimates of the two components of the gradient $(\hat{I}_x, \hat{I}_y)$.

2. Compute the magnitude of the surface normal

$$|\nabla g| = \sqrt{1 + \hat{I}_x^2 + \hat{I}_y^2}$$

3. Apply the filter kernel to the current image

$h_1 = \dfrac{1}{8\,\lvert\nabla g\,(x_0-1, y_0-1)\rvert}$	$h_2 = \dfrac{1}{8\,\lvert\nabla g\,(x_0, y_0-1)\rvert}$	$h_3 = \dfrac{1}{8\,\lvert\nabla g\,(x_0+1, y_0-1)\rvert}$
$h_4 = \dfrac{1}{8\,\lvert\nabla g\,(x_0-1, y_0)\rvert}$	$h(x_0, y_0) = 1 - \sum_{i=1}^{8} h_i$	$h_5 = \dfrac{1}{8\,\lvert\nabla g\,(x_0+1, y_0)\rvert}$
$h_6 = \dfrac{1}{8\,\lvert\nabla g\,(x_0-1, y_0+1)\rvert}$	$h_7 = \dfrac{1}{8\,\lvert\nabla g\,(x_0, y_0+1)\rvert}$	$h_8 = \dfrac{1}{8\,\lvert\nabla g\,(x_0+1, y_0+1)\rvert}$

4. Iterate as needed by returning to step 1.

6 Nonlinear Dynamics of an Edge

We study experimentally the dynamics of MCD when applied to edges as we proceed forward in time, to verify the theoretical findings of Section 2 and to demonstrate the adequacy of the discrete implementation derived in Section 5.

6.1 Invariance and Developed Enhancement

The MCD algorithm was applied to the edge model of Fig. 1. The noise free original edge and the output after 80 iterations are shown superimposed in Fig. 2 (bottom left). To understand this result we recall the shape of the mean curvature of the original edge shown in Fig. 1, and bear in mind the most essential property of MCD, that of the spatial averaging of mean curvature. The two pulses in Fig. 1 correspond to the mean curvature at the two shoulders of the ramp. Diffusion occurs only at the shoulders since only there is H nonzero, while *at* the edge, diffusion is halted since H vanishes, leading to edge invariance. The behavior at both shoulders is identical, and we will thus describe only the behavior of the upper. This shoulder is surrounded on each side with

regions of zero mean curvature. From the right it is the flat region resulting from the leveling off. From the left it is the plane region where the edge lies. These two regions of zero mean curvature try to push the curvature at the shoulder from both sides to zero, and simultaneously diffusion is halted in these two regions since H is zero. This push and the simultaneous halt of the diffusion results in the pulse becoming impulsive (loss of spatial support and a higher magnitude), and also in its shifting. These dynamics obtained *experimentally* are shown in Fig. 2. Notice that the shift is inwards towards the edge location. The reason behind the shift being inward is that the extent of the flat region is larger than the span of the edge, which follows from the definition of an edge.

[Figure 2 about here.]

The experimental discrete data shown in Fig. 2 indicates that at time 80 the mean curvature is zero almost everywhere and the nonzero mean curvature has a spatial width of 1 pixel, a pulse that can longer be diffused since it is surrounded by vanishing mean curvature of spatial support larger than or equal to the kernel size (3×3). At this state the algorithm converges and the surface becomes invariant to the diffusion process. Note that this state corresponds to three planes intersecting in straight lines (the mesh in Fig. 2), it is evident that these three planes are an enhanced version of the original edge with an intact location. This developed enhancement can also be seen in the reduction of the edge's span as displayed by the discrete mean curvature graphs shown in Fig. 2.

The dynamics of the magnitude of the surface gradient are similar to those of the mean curvature, in that this magnitude rises with time and maintains accurate edge location. This rise in magnitude is another indication of the developed enhancement.

6.2 Noisy Edge

The MCD algorithm was applied to a noisy version of the edge model of Section 6.1. The original edge with zero-mean additive white Gaussian noise with standard deviation of 30 (SNR of about 8dB) is shown in the first element of Fig. 3. As can be seen this noisy edge is a rough surface of high mean curvature. The MCD algorithm quickly averages the mean curvature creating smoother patches (lower mean curvature), and as we iterate we bring more spatial context to bear on the averaging process resulting in larger and smoother patches. The reduction of mean curvature occurs progressively on small patches. First a small patch becomes smoother, then eventually planar, and

finally joining other small planar patches to form planes.

[Figure 3 about here.]

Local high mean curvature characterizes noise, and as it is locally averaged by the algorithm, the ramp edge is gradually revealed. The ramp is also undergoing mean curvature averaging, which leads to enhancement with the edge location intact. The dynamics of this averaging of the underlying ramp are identical to that of the noise free edge presented in Section 6.1. The state of convergence (not shown in Fig. 3) is identical to the noise free case shown in Fig. 2 (bottom left). The algorithm completely removes the additive noise, and enhances the edge without affecting the edge locality.

7 Applications

To demonstrate the properties of the MCD algorithm of Section 5 it was used in two image processing applications: image noise removal and transparent coding.

7.1 Image Noise Removal

To demonstrate the capability of the algorithm to remove noise while preserving structure, it was applied to a moderately noisy gray scale image. A high quality image was chosen and zero mean white Gaussian noise was added to produce a noisy test image. The noise variance was estimated from a flat region of each image, following the suggestion in [22] that such an estimate is best obtained from the difference between the image and a low pass filtered version of the image. The low pass filter applied was a 3×3 uniformly weighted averaging filter. A peak signal-to-noise (PSNR) was computed for each image.

In Table 1, the noise variance and PSNR are given for the original and noisy images and for the images produced by four and ten iterations of the MCD algorithm. The PSNR dropped by 12 dB after noise addition, but was nearly 10 dB above that of the original image after only four iterations and nearly 20 dB above after ten iterations.

[Table 1 about here.]

The original image, the noise-added image, and the results of four and ten iterations of MCD processing are shown in Figure 4. Since the effects of the processing can be difficult to perceive in

a half-tone rendition, edge maps of these images, with a fixed edge gradient threshold, are shown in Figure 5. Note the excellent preservation of edges in the processed images.

[Figure 4 about here.]

[Figure 5 about here.]

7.2 Application to Perceptually Transparent Coding

In perceptually transparent image coding, the coding algorithm is designed such that the coding errors are not visible to a human observer. The transparent coding algorithms discussed in [23] are intended for application to high quality images having very high SNR. The compression ratio of such algorithms is improved by first filtering the image to remove non-visible noise and fine structure. This preprocessing filter must not induce any observable distortion.

Potential filtering algorithms evaluated quantitatively and qualitatively included: median, Lee additive [24], gradient inverse weighted smoothing [25], maximum homogeneity [26], edge and line weights [27], sigma [28], anisotropic diffusion with a Gaussian kernel (ADG) and a Cauchy kernel (ADC) [1], and MCD. The median filter, anisotropic diffusion algorithms and the MCD algorithm were found to provide the best performance.

Care was taken in the evaluation so that the number of iterations of each algorithm was chosen so that no visible distortion was introduced. This was done by applying the MCD algorithm, viewing at a distance of six times the image height, and having several observers agree that no changes were introduced. The other algorithms were adjusted by comparing their results displayed in pseudo-color, where all changes, both visible and non-visible in the gray-scale image, could be observed.

This evaluation was performed on three images: the well-known Lena image, a busy aerial image, and the bicycle image of Section 7.1. The variances of the original and processed images are given in Table 2. For each image, the MCD algorithm provided the greatest decrease in image variance. The ratio of processed to initial variance differs by over two orders of magnitude for the three images, with the greatest decrease achieved on the bicycle image and the least on the aerial image. It appears that this is directly related to the degree of structure in the image.

[Table 2 about here.]

8 Conclusions

The representation of an image as a surface provides the basis for the development of a new formulation for inhomogeneous diffusion, in which the diffusion coefficient is the inverse of the magnitude of the surface normal and the image surface evolves with a speed proportional to the mean curvature. This averaging preserves image edges, as their mean curvature is zero, while noise is averaged since it has high mean curvature.

References

[1] P. Perona and J. Malik, "Scale-space and edge detection using anisotropic diffusion," *IEEE Trans. Pattern Anal. Machine Intell.*, vol. PAMI-7, pp. 629–639, 1990.

[2] L. Alvarez, P. L. Lions, and J. M. Morel, "Image selective smoothing and edge detection by nonlinear diffusion II," *SIAM J. Numer. Anal.*, vol. 29, pp. 845–866, June 1992.

[3] B. B. Kimia and K. Siddiqi, "Geometric heat equation and nonlinear diffusion of shapes and images," in *Proc. IEEE Computer Vision and Pattern Recognition Conf.*, pp. 113–120, June 1994.

[4] L. I. Rudin, S. Osher, and E. Fatemi, "Nonlinear total variation based noise removal algorithms," *Physica D*, vol. 60, pp. 259–268, 1992.

[5] G. Sapiro, A. Tannenbaum, Y. L. You, and M. Kaveh, "Experiments on geometric image enhancement," in *Proc. IEEE Int. Conf. on Image Processing*, vol. 2, pp. 472–476, Nov. 1994.

[6] G. Sapiro and A. Tannenbaum, "Area and length preserving geometric invariant scale-spaces," *IEEE Trans. Pattern Anal. Machine Intell.*, vol. PAMI-17, pp. 67–72, 1995.

[7] B. Romeny, ed., *Geometry Driven Diffusion in Computer Vision.* Kluwer, 1994.

[8] A. I. El-Fallah and G. E. Ford, "Nonlinear adaptive image filtering based on inhomogeneous diffusion and differential geometry," in *Proc. SPIE*, vol. 2182, pp. 49–63, 1994.

[9] A. I. El-Fallah and G. E. Ford, "The evolution of mean curvature in image filtering," in *Proc. IEEE Int. Conf. on Image Processing*, vol. 1, pp. 298–302, 1994.

[10] L. C. Evans and J. Spruck, "Motion of level sets by mean curvature I," *J. Differential Geometry*, vol. 33, pp. 635–681, 1991.

[11] M. G. Crandall and P. L. Lions, "Viscosity solutions of Hamilton-Jacobi equations," *Trans. Amer. Math. Soc.*, vol. 277, pp. 1–42, 1983.

[12] M. G. Crandall, L. C. Evans, and P. L. Lions, "Some properties of viscosity solutions of Hamilton-Jacobi equations," *Trans. Amer. Math. Soc.*, vol. 282, pp. 487–502, 1984.

[13] P. L. Lions, "Optimal control of diffusion processes and Hamilton-Jacobi-Bellmam equations I," *Comm. Partial Differential Equations*, vol. 8, pp. 1101–1134, 1983.

[14] K. Ecker and G. Huisken, "Mean curvature evolution of entire graphs," *Annals of Mathematics*, vol. 130, pp. 453–471, 1989.

[15] K. Ecker and G. Huisken, "Interior estimates for hypersurfaces moving by mean curvature," *Inventiones Mathematicae*, vol. 105, pp. 547–569, 1991.

[16] O. A. Ladyzhenskaya, V. A. Uraltseva, and N. N. Uraltseva, "Linear and quasilinear equations of parabolic type," *Transl. Math. Monographs AMS*, vol. 23, 1968.

[17] M. A. Grayson, "A short note on the evolution of a surface by its mean curvature," *Duke Math. J.*, vol. 68, pp. 555–558, 1989.

[18] K. Hollig and J. Nohel, "A diffusion equation with a non-monotone constitutive function," in *Systems of Nonlinear Partial Differential Equation* (J. Ball, ed.), pp. 409–422, Boston, MA: Reidel, 1983.

[19] F. Catte, P. L. Lions, J. M. Morel, and T. Coll, "Image selective smoothing and edge detection by nonlinear diffusion," *SIAM J. Numer. Anal.*, vol. 29, pp. 182–193, February 1992.

[20] M. Protter and H. Weinberger, *Maximum Principles in Differential Equations.* Prentice-Hall, 1967.

[21] A. Rosenfeld and A. C. Kak, *Digital Picture Processing*, vol. 2. Academic Press, Inc., second ed., 1982.

[22] S. I. Olsen, "Estimation of noise in images: An evaluation," *Comput. Vision Graphics Image Processing*, vol. 55, pp. 319–323, 1993.

[23] V. R. Algazi, T. R. Reed, G. E. Ford, E. Maurincomme, I. Hussain, and R. Potharlanka, "Perceptually transparent coding of still images," *IEICE Trans. Communications*, vol. E75-B, no. 5, pp. 340–348, 1992.

[24] J. S. Lee, "Refined filtering of image noise using local statistics," *Comput. Graphics Image Processing*, vol. 15, pp. 380–389, 1981.

[25] D. C. Wang, A. H. Vagnucci, and C. C. Li, "Gradient inverse weighted smoothing scheme and the evaluation of its performance," *Comput. Graphics Image Processing*, vol. 15, pp. 167–181, 1981.

[26] F. Tomita and S. Tsuji, "Extraction of multiple regions by smoothing in selected neighborhoods," *IEEE Trans. Syst., Man, Cybern.*, vol. 8, pp. 107–109, 1977.

[27] A. Lev, S. W. Zucker, and A. Rosenfeld, "Iterative enhancement of noisy images," *IEEE Trans. Syst., Man, Cybern.*, vol. 7, pp. 435–442, 1977.

[28] J. S. Lee, "Digital image smoothing and the sigma filter," *Comput. Graphics Image Processing*, vol. 24, pp. 255–269, 1981.

List of Figures

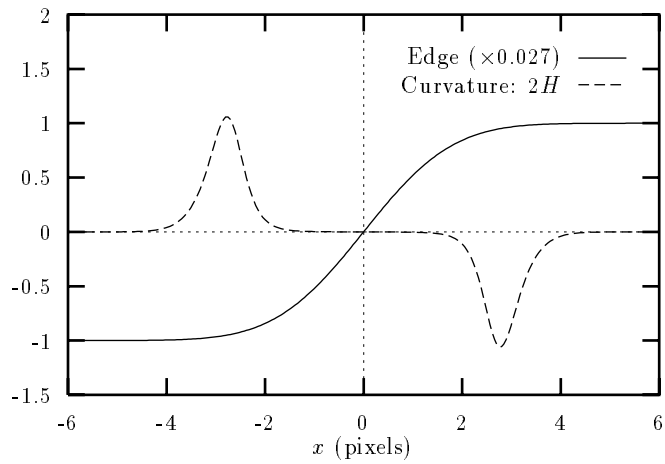

Figure 1: Gaussian blurred edge and its mean curvature.

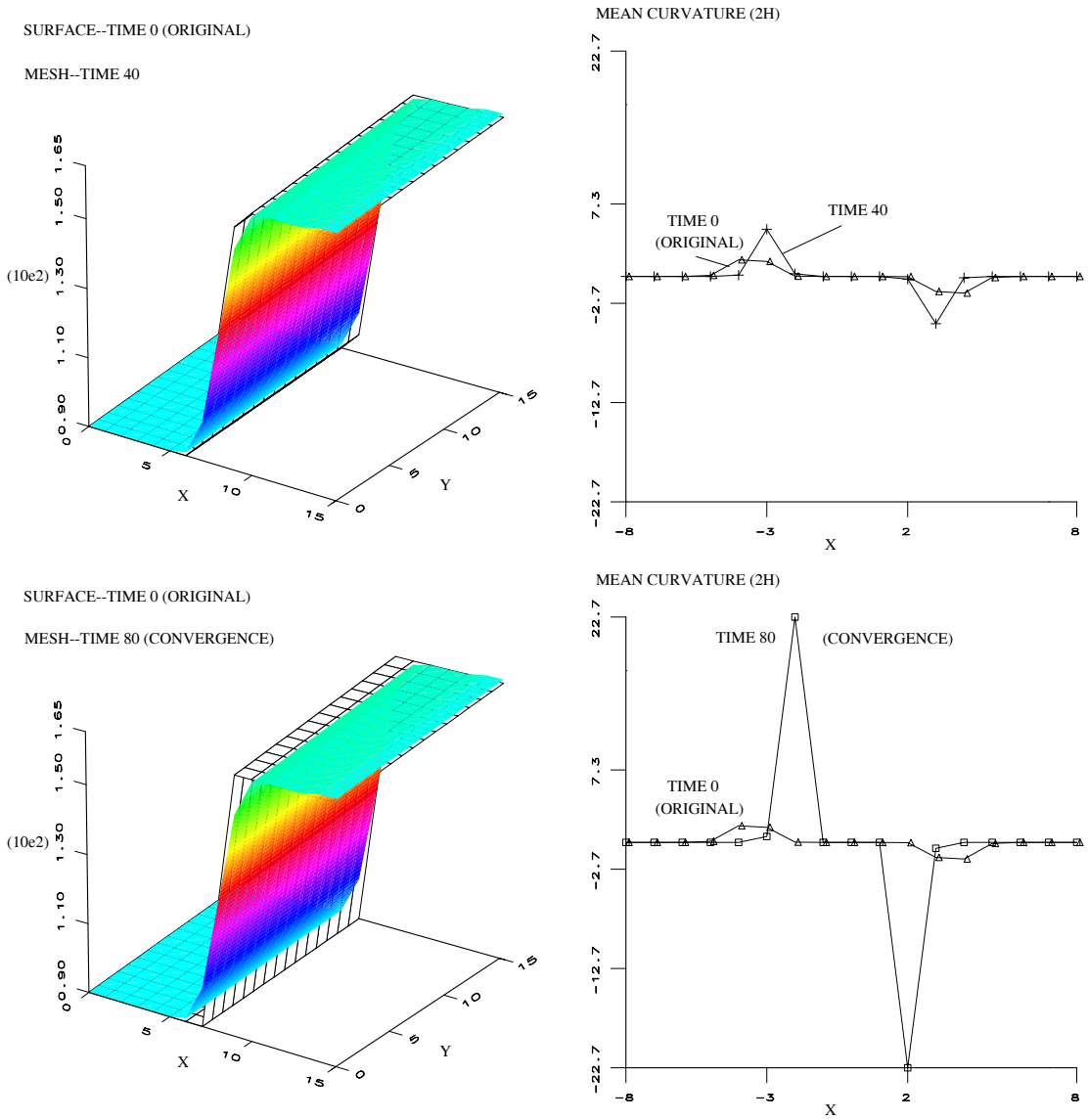

Figure 2: Mean curvature dynamics and the corresponding surfaces.

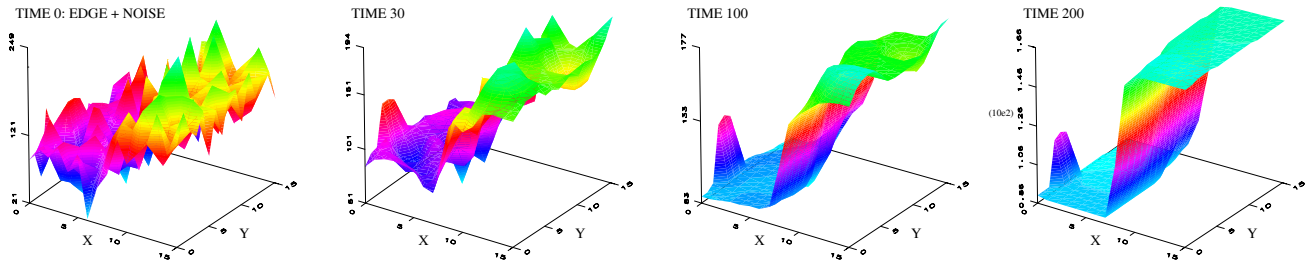

Figure 3: Evolution of the noisy edge surface under mean curvature diffusion

Figure 4: Top: Original image (left), noise-added image (right); Bottom: MCD filtered output images, iterations four (left) and ten (right)

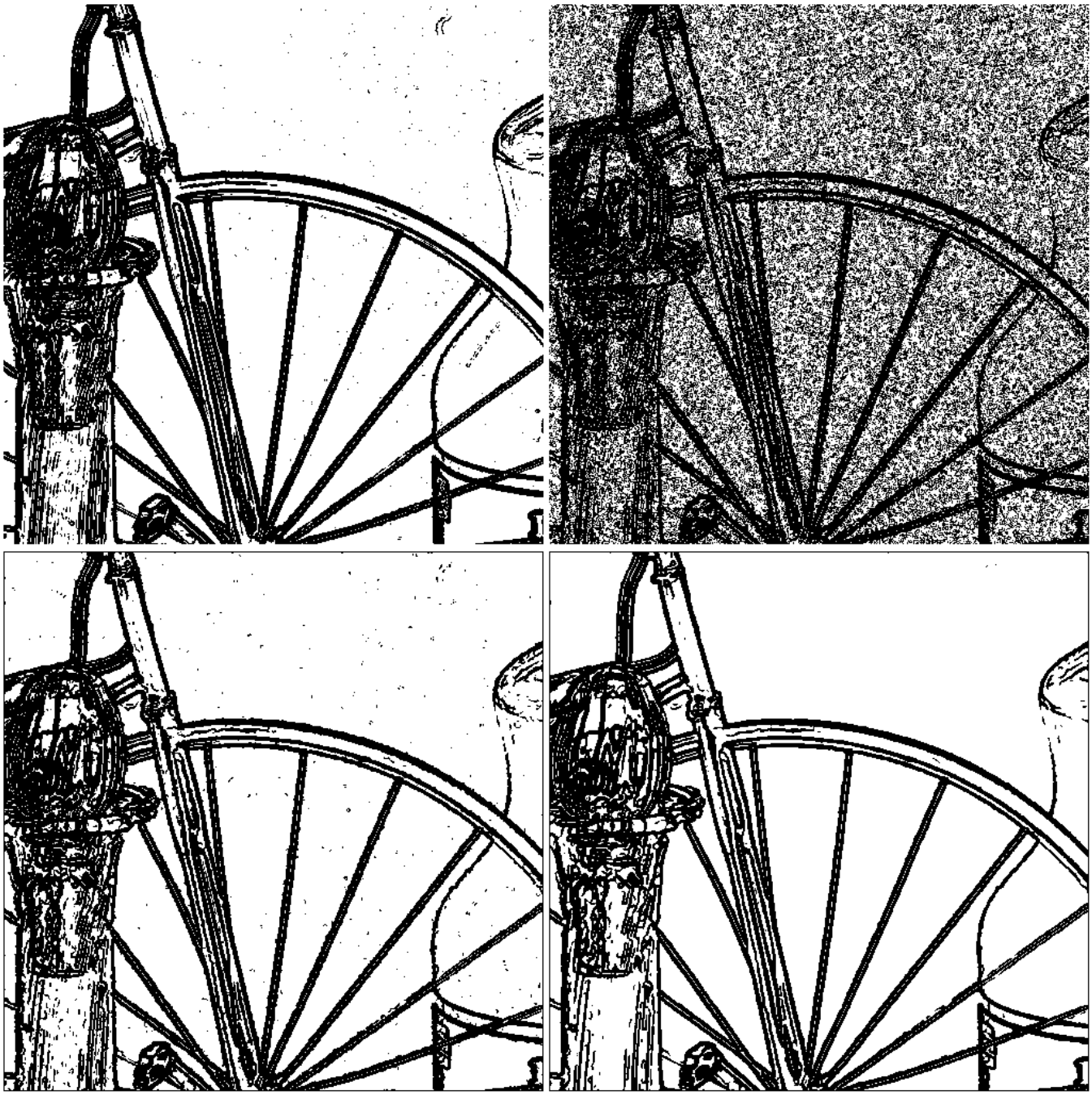

Figure 5: Edge maps of images in Figure 4

List of Tables

Image	Variance	PSNR
Original	1.2757	45.99
Noisy Input	24.0227	34.01
Iteration 4	0.1867	54.97
Iteration 10	0.0173	65.22

Table 1: Quantitative performance of the MCD algorithm

Image	Lena	Aerial	Bicycle
Original Variance	5.9080	1.1805	1.4515
Median	0.5093	0.1895	0.1034
ADG	0.0746	0.4551	0.0036
ADC	0.0431	0.2287	0.0037
MCD	0.0229	0.0655	0.0004

Table 2: Comparison of noise variance reductions